doi:10.14311/ppt.2019.2.140
Plasma Physics and Technology **6**(2):140–143, 2019

ARC BEHAVIOURS IN THE HV SF_6 GAS-BLAST INTERRUPTER

S. Averyanova*, E. Tonkonogov

Institute of Energy and Transport System, Peter the Great St. Petersburg Polytechnic University, 29, Polytechnicheskaya st., St. Petersburg, 195251, Russia

* averly@yandex.ru

Abstract. A comprehension of the dielectric strength recovery processes during the interruption of short-circuit currents in the high-voltage SF_6 gas-blast circuit breakers is necessary for their modernisation in order to increase the rated voltage and short circuit breaking current per one break. This paper presents numerical results of the turbulence effects on the interruption ability in the SF_6 extinguishing arc chamber.

Keywords: dielectric strength recovery, turbulence, nozzle geometry, SF_6 circuit breaker.

1. Introduction

The breakdown probability during the interruption mode increases with increasing the rated voltage. It is necessary to reach a good comprehension of physical processes occurring in high-voltage (HV) gas-blast circuit breakers (CBs) during the interruption mode for solving the above mentioned problem. It is possible to distinguish four phases of the dielectric strength recovery after the current zero [1].

The first phase is related to the thermal mode. The hot-gas channel remains conductive. The thermal balance between heating and cooling processes, primarily due to the turbulent dissipation in the nozzle throat, plays the important role during this mode. This mode lasts several µs [1].

The second phase is related to the dielectric mode. For this mode, the volume of the hot-gas channel is negligible in the downstream zone of the insulation nozzle, but in the upstream zone of the nozzle there is a considerable amount of hot-gas portions, especially in the stagnation zone. As well known, the thermal clogging is used for the additional pressure rise during the interruption process in the puffer-type HV gas-blast CB. On the one hand, the pressure rise helps to increase this interruption ability. On the other hand, the temperature in the compression volume increases too, and this leads to reduction in the upstream dielectric strength. Indeed, the experimental data [1, 2] show that the presence of conducting gas in the upstream zone of the nozzle may lead to the breakdown in the vicinity of the u_1 point (the four-parameter reference line for the transient recovery voltage (TRV)) for BTF (the breaker terminal fault 100%) [3]. At the same time, the experimental data [4] for the puffer-type CB with rated parameters of 50 kA, 300 kV (u_1=239 kV, t_1=119 µs [3]), and insulation nozzle throat diameters d = 35, 40 (= d_0, Fig. 1), 45 mm show a clear correlation between dielectric strength recovery and insulation nozzle throat diameter. This correlation is nonlinear, and the smaller nozzle diameter leads to the worst interruption ability.

The third phase is related with the additional gas heating due to recombination effects. The turbulent kinetic energy and the dielectric strength in the upstream zone are increasing rapidly during this mode, but there is a probability of the breakdown through the stagnation zones.

The final phase begins after ending the recombination. The dielectric strength is related to that of cold gas.

This paper analyses the arc and flow interface parameters that may influence the puffer-type HV SF_6 CB interruption ability in the vicinity of the u_1 point (between the 2nd and the 3rd modes) for different diameters of the insulation nozzle throat.

2. Mathematical Simulation

Fig. 1 shows the schematic diagram of the puffer-type HV SF_6 CB that was used for the numerical simulation and the computational domain is plotted with dotted lines.

The insulation throat diameter varies within $d = (0.85 - 1.15)d_0$. The diameter of the metal nozzle throat, d_m, is 2 mm smaller than that of the insulation nozzle throat. The rated pressure is equal to p_0 = 7 atm. The current is changing with time according to the synthetic test with the stationary value I_{max} = 2.5 kA, and dI/dt = -17.7 A µs^{-1}.

For numerical analysis of the insulation throat diameter impact on the dielectric strength recovery, the time-averaged system of equations was used, including the Navier-Stokes equations, the continuity and energy equations [5]. The Ohm law, models of the turbulent viscosity and radiation transfer are added to the system of differential equations.

The turbulence model for the steady state analysis takes into account the turbulence effects in the shear layer between arc and gas flow produced by two types of instability: both the shear instability and Rayleigh-Taylor instability [5]. For the unsteady state analysis, the "freeze"-theory for the kinematic turbulent viscosity, ν_t, was used [5]. It means that at all moments

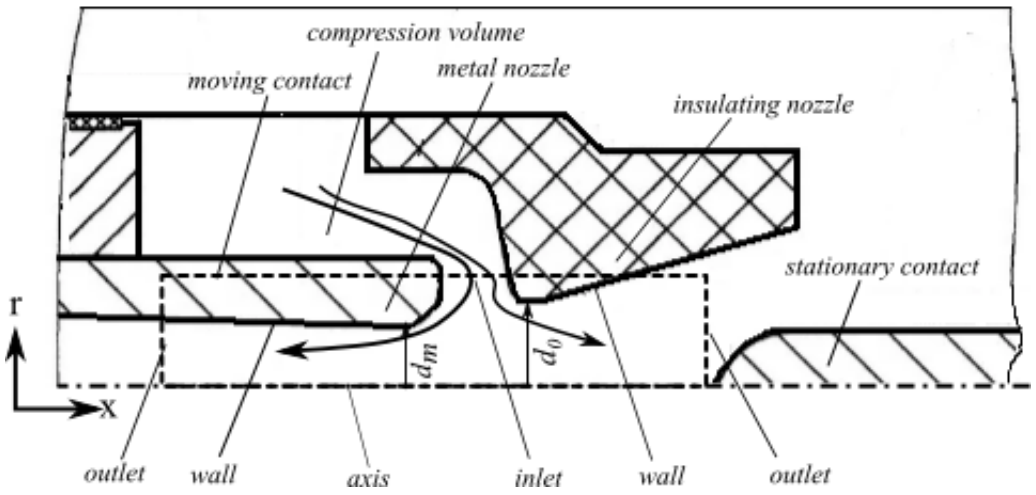

Figure 1. The simplified geometry and the computational domain of the puffer-type SF_6 CB.

of time when the current is rapidly falling down, the kinematic turbulent viscosity is assumed constant and its numerical value is equal to its stationary value. The dynamic coefficient of the turbulent viscosity, μ_t, comprises the geometric mean density calculated in terms of the point density and that of the cold gas in this section. When the current is falling down, the arc density and the turbulent viscosity are growing after the current zero.

For the radiation transfer, the "radiation conductivity"approximation was used [6]. The radiation transfer plays an important role in the heat transfer at the maximum current, but it does not matter after the current zero.

As known from experiments [7], after the current zero there is the post-arc part where the temperature is falling down more quickly than in other parts. Therefore, we may assume that the gas dielectric strength will start to recover if the temperature on the arc axis reaches values of 3000 K at least at two points [8].

For the numerical simulation, the home-made 2D CFD code was used based on the algorithm given in [9] together with the convective fluxes approximation by Roe's method [10, 11]. The gas material functions are computed based on the data given in [8]. The boundary conditions are presented in Fig. 1. The unsteady state simulation time is equal to 300 µs, including the current falldown 141 µs period and dielectric strength recovery 159 µs period. Based on the experimental pressure curves [12, 13], the inlet static pressure assumed constant during the simulation. The walls ablation and its influence on the pressure in the compression volume is not considered in this simulation.

3. Results and Discussion

Results of the numerical simulation are presented in Figs. 2–5. So, considered is the influence of the arc and flow interface parameters on the dielectric strength recovery in the vicinity of the u_1 point. Tested are three moments of time related to the stationary arc parameters (-141 µs), the thermal breakdown phase (3 µs), and the dielectric breakdown phase in the vicinity of the u_1 point (119 µs).

Fig. 2 shows the normalised turbulent viscosity (the ratio of turbulent viscosity, μ_t, to the maximum value of μ_t at d_0 and -141 µs) as the function of the normalised radial coordinate, r/d_0, for the insulation nozzle throat at the steady state of the arc and flow. Obviously, the geometry with insulation nozzle throat being equal to $0.85\,d_0$ ensures the largest of the turbulence viscosity in the shear layer between the arc and flow. The difference between maximum values on the curve of this figure and those related to the insulation nozzle throat diameter being equal to d_0 is about 40%. The maximum value of the turbulent viscosity, μ_t, decreases with increasing the nozzle throat diameter. It is due to the decrease in the pressure ratio leading to the decrease in the shear instability component of the turbulent viscosity, μ_t.

The difference between nozzle throat diameters $0.85\,d_0$ and d_0 remains equal to about 40% at all moments of time. After the current zero, the value of the turbulent viscosity for $d > d_0$ increases more slowly than for $d \leqslant d_0$, and is practically independent of the nozzle throat diameter. This is due to the small value of the turbulent viscosity in the shear layer between the arc and flow. It means that after the current zero the turbulent heat transfer is weak and the temperature falls down (while the density grows up) more slowly than for geometries with $d \leqslant d_0$.

Fig. 3 shows the normalised turbulent viscosity (the ratio of turbulent viscosity, μ_t, to the maximum value of μ_t at d_m and -141 µs) as the function of the normalised radial coordinate, r/d_0, for the metal nozzle throat at the steady state of the arc and flow. Obviously, the turbulent viscosity in the metal nozzle throat reveals the same behaviour as in the insulation one. The difference between $0.85\,d_0$ and d_0 nozzle throat diameters is equal to about 33% at all mo-

ments of time. After the current zero, the value of the turbulent viscosity for $d > d_0$ increases more slowly than for $d \leqslant d_0$ and is practically independent of the nozzle throat diameter similar of the insulation nozzle throat.

Fig. 4 shows the average temperature on the axis, $T_{\text{axis, mid}}$, as the function of time, t. The maximum temperature relates to the maximum nozzle diameter, $1.15\,d_0$. In [7] it is shown, that the arc radius is in the inverse relationship to the pressure. For the geometry considered, the pressure is smaller and the arc radius is maximum in all presented geometries. Considering that the synthetic test is used, the Joule heating is the same for all cases. Therefore, the lowest temperature is reached when the arc radius is largest. However, it should be noted that the steady-state temperature for all geometries are about 18000 K, that is consistent with the experimental data [7]. In the vicinity of the current zero the average axial temperature is about 10000 K, except for the $1.15\,d_0$ insulation nozzle throat diameter. The minimum turbulent viscosity in this nozzle is related to the weak decay of the conductivity in the post-arc channel. Moreover, in this case, the pressure ratio is less than the critical value for this geometry, and the convective heat transfer is weaker than in other computations. In the vicinity of the u_1 point all curves show temperatures smaller than 3000 K, except for the $1.15\,d_0$ insulation nozzle throat diameter. It means that the most part of the gas on the axis is non-conductive, but gas conductivity zones exist near the outlet boundaries in the computational domain.

Fig. 5 shows the normalised radius of the conductivity zone in the insulation nozzle throats (the ratio of the conductivity zone radius, r_{cond}, to that for the insulation nozzle throat diameter, $r_{\text{cond}}(d_0)$, at every moment of testing) as the function of the normalised insulation nozzle throat diameter, d/d_0. This figure presents only two curves because in several microseconds the temperature in the insulation nozzle reaches 3000 K and the gas becomes non-conductive. The maximum radius is related to the $1.15\,d_0$. Moreover, the falldown rate for $d > d_0$ is smaller than that for $d \leqslant d_0$.

Considering the above mentioned, we assume that the minimum diameter ($0.85\,d_0$) ensures the best arc and flow interface parameters for arc interruption and dielectric strength recovery. Nevertheless, this analysis does not take into account the wall ablation. The arc radiation is very intensive at the current peak in the HV CB [4]. The reduction in the nozzle throat diameter leads to the increase in the thermal clogging time. The long-time clogging leads to the nozzle wall erosion and the increase in the nozzle throat diameter due to the long-time arc filling of the nozzle. Therefore, the gas high temperature in the compression volume may lead to the slower falldown of the post-arc temperature and the increase in the breakdown probability [4]. The approximate estimate [7]

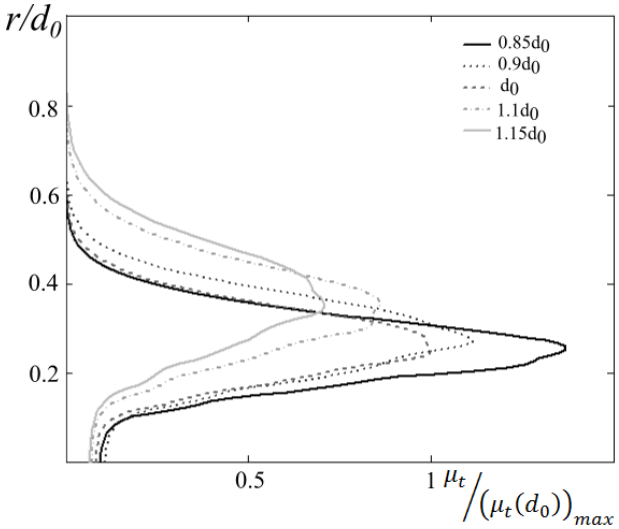

Figure 2. The normalised turbulent viscosity as the function of the normalised radial coordinate for the insulation nozzle throat at the steady state flow.

gives the arc radius about 35 mm for simulations. In this case, the thermal clogging can be strong enough, that is confirmed by the data [4]. Therefore, it may be assumed that the insulation nozzle throat diameter should exceed the arc radius by 10–15%. In this range of throat diameters, the thermal clogging ensures the pressure ratio leading to the flow conditions under which the arc interruption is successfully fulfilled. On the other hand, the temperature rise in the compression volume due to the nozzle clogging has no significant effect on the dielectric strength recovery. If the nozzle diameter exceeds this range, the pressure rise in the compression volume is not great enough to ensure the successful arc interruption.

4. Conclusions

The numerical analysis shows that the arc interruption and dielectric strength recovery in the puffer-type HV CB (BTF 100%) are closely related to the arc and flow interface parameters, which ensures the dominant cooling mechanisms, such as turbulent and convective heat transfer. The above mentioned range of the insulation nozzle throat diameter range may be used when we provide arc and flow interface conditions for successful arc interruption. In this paper, the wall ablation was not taken into account, but this is one of the causes of the breakdown through the wall boundary layer with the rated voltage per one break increasing in the puffer-type HV CB. When considering the impact of the insulation nozzle ablation on the dielectric strength recovery it will help us to predict BTF 100% test results more qualitatively.

References

[1] E. Schade. Similarity of the dielectric recovery characteristic of axially blown arcs in SF_6. In *Proc. 8-th Conf. on Gas Discharges, Oxford*, pages 50–53, 1985.

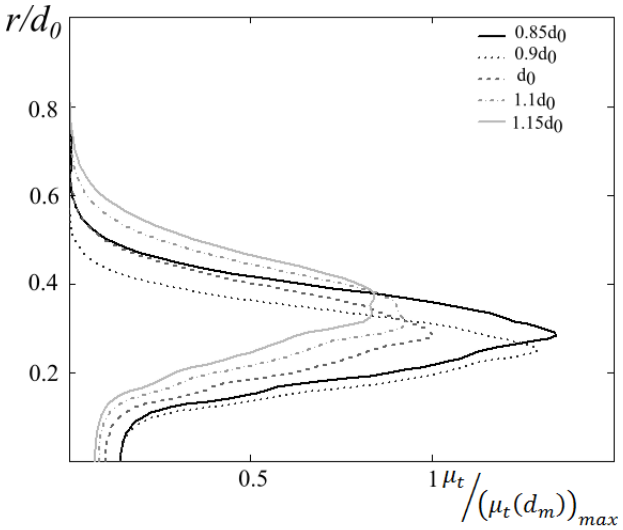

Figure 3. The normalised turbulent viscosity as the function of the normalized radial coordinate for the metal nozzle throat at the steady state flow.

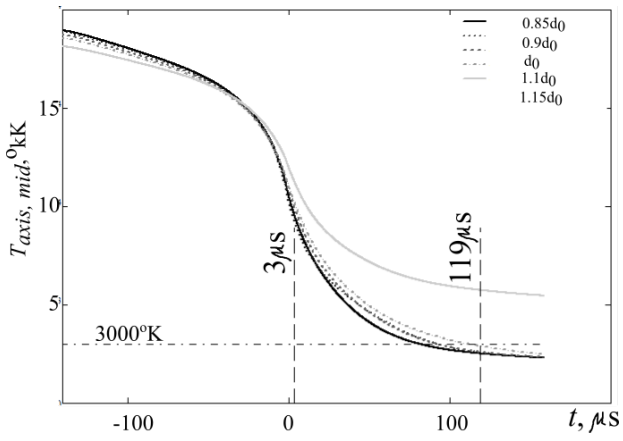

Figure 4. Average axial temperature as the function of time.

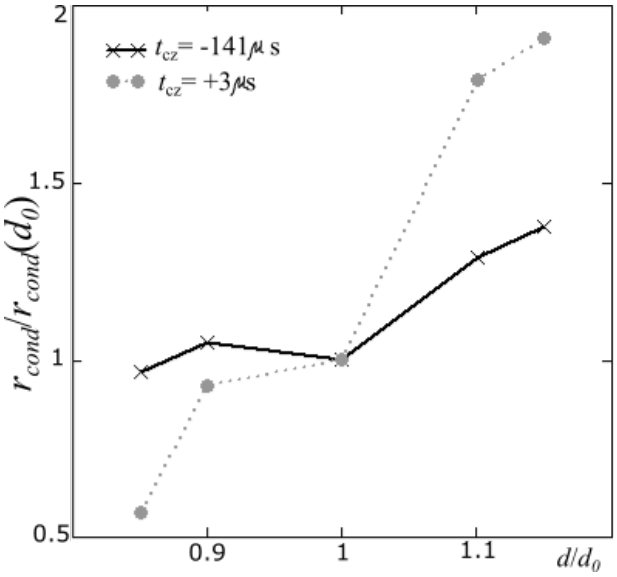

Figure 5. The normalised radius of the conductivity zone in the insulation nozzle throats as the function of the normalised insulation nozzle throat diameter.

Switching Arc, Brno (Czech Republic), volume 1, pages 3–6, 22-26 Sept., 2003.

[7] K. Ragaller (editor). *Current interruption in high voltage networks.* Plenum Press, NewYork, 1978.

[8] L. S. Frost and R. W. Liebermann. Composition and transport properties of SF_6 and their use in a simplified enthalpy flow arc model. *Proceedings of the IEEE*, 59(4):474–485, 1971. doi:10.1109/PROC.1971.8206.

[9] R. M. Beam and R. F. Warming. An implicit factored scheme for the compressible Navier-Stokes equations. *AIAA Journal*, 16:393–401, 1978. doi:10.2514/3.60901.

[10] P. L. Roe. Approximate Riemann solvers, parameter vectors and difference scheme. *J. Comput. Phys.*, 43:357–372, 1981. doi:10.1016/0021-9991(81)90128-5.

[11] C. Hirsch. *Numerical Computation of Internal and External flows, v.2.* Wiley, 1990.

[12] A. Kornhaas, F. Reichert, C. Leu, and F. Berger. Simulation of interaction between switching arc and switching mechanics in SF_6 self-blast circuit breakers. In *XVIII Symp. on Physics of Switching Arc, Brno (Czech Republic)*, pages 276–279, 7-11 Sept., 2009.

[13] J. Zhong, Z. Li, and Y. Guo. Pressure and arc voltage measurements in a 252 kV SF_6 puffer circuit breaker. In *XXth Symp. on Physics of Switching Arc, Brno (Czech Republic)*, volume Contributed Papers, pages 332–335, 2-6 Sept., 2013.